PPPL--3219

Simulation of α-Particle Redistribution due to Sawteeth on TFTR

Yi Zhao, Roscoe B. White

Princeton Plasma Physics Laboratory

P.O. Box 451, Princeton, New Jersey 08543-0451

Abstract

In recent Deuterium-Tritium experiments on the Tokamak Fusion Test Reactor(TFTR), both the Pellet Charge Exchange (PCX) [*Phys. Rev. Lett.* **75**, 846 (1995)], [*Nucl. Fusion* **35**, 1437 (1995)] and the alpha Charge Exchange Recombination Spectroscopy (α-CHERS) [*Phys. Rev. Lett.* **75**, 649 (1995)] diagnostics indicate that sawtooth oscillations can cause significant broadening of the fusion alpha radial density profile. We investigate this sawtooth mixing phenomenon by applying a Hamiltonian guiding center approach. A model of time evolution of the Kadomtsev-type sawtooth [*Sov. J. Plasma Phys.* **1**, 389 (1976)] is constructed. The presence of more than one mode in the nonlinear stage of the sawtooth crash is necessary to cause significant broadening of the alpha density profile. Use of numerical equilibria allows us to perform detailed comparisons with TFTR experimental data. Our results are in reasonable agreement with α-CHERS and show a broadening of alpha particles similar to that seen in PCX measurements.

DISCLAIMER

PACS number: 52.20.Dq, 52.35.Py,

I. Introduction

In recent D-T experiments on the Tokamak Fusion Test Reactor (TFTR),[1] diagnostics including Pellet Charge Exchange (PCX)[2–4] and Alpha Charge Exchange Recombination Spectroscopy (α-CHERS)[5] have been used to measure the radial density profile of confined α particles. Results from these measurements indicate that sawtooth instabilities can transport a significant number of alphas from the core-region into the outer region ($r/a \geq 0.3$). The observed sawtooth mixing is an issue of fundamental importance for two reasons. First, it can reduce the alpha heating in the central region where it is most efficient for sustaining the fusion reaction. Second, it can enhance alpha particle losses by redistributing a fraction of the alphas onto first-orbit loss or ripple-loss orbits, thus reducing the total alpha-heating available to the bulk plasma, and producing an excessive heat load to the wall.

The model we present here adopts a fundamental approach by following the particle guiding center motion during a whole sawtooth crash cycle. It differs from previous analytic or empirical models[6–8] in that it automatically takes into account the effects of finite orbit width and toroidal drift. In some experiments, the width of fast ion orbits is comparable to that of the sawteeth region. Furthermore, alpha particle energy modification due to the time varying fields is essential to explain the redistribution of deeply trapped α particles. The Monte Carlo method is used to generate particles representing the alpha distribution (peaked) just before the sawtooth crash. The fact that more than one poloidal harmonic is needed to cause significant broadening of the alpha density profile indicates the important role the stochasticity of magnetic field

lines plays in this process. Since the PCX diagnostic only detects deeply trapped particles within a very narrow range (± 0.001) of pitch angle around $v_\parallel/v = -0.048$, the simulation and comparison with experiment becomes more subtle. In this case, field line stochasticity is not sufficient to explain the data. We also need to introduce the electric field which is non-negligible during the sudden crash. It is this electric field that causes the particle diffusion in pitch angle and energy space. The electric field parallel to **B** is zero due to the rapid response of the electrons, so energy is changed only by the field perpendicular to **B** through cross field drift. Thus trapped particles, with larger drift motion, are more strongly affected. Ripple effects are not considered since the measured alpha loss rates[9] were not changed significantly ($< 1\%$) during the sawtooth crashes, indicating that in these experiments the sawtooth mixing results in only an internal redistribution of α particles with no induced loss.

In Sec. II we briefly describe the guiding center equations used for following particle trajectories. The models for the sawtooth mode structure, the evolution of the sawtooth crash and the particle distribution are given in Sec. III, V and VI. The simulation results and comparison with experimental measurements are presented in Sec. VII.

II. Hamiltonian Guiding Center Equations

The Hamiltonian guiding center equations,[10–12] allow very efficient numerical evaluation of particle trajectories for times long enough to investigate fast ion transport during sawtooth crashes. Since the particle's drift motion is described by a set of

canonical variables which are closely related to the magnetic coordinates, this formulation is convenient for plasmas with arbitrarily shaped cross sections. The contravariant and covariant forms of the equilibrium field are:

$$\mathbf{B} = \nabla\zeta \times \nabla\psi_p + q\nabla\psi_p \times \nabla\theta \tag{1}$$

$$\mathbf{B} = g\nabla\zeta + I\nabla\theta + \delta\nabla\psi_p \tag{2}$$

with ψ_p the poloidal flux, θ the poloidal angle, and ζ the toroidal angle. For low β plasmas with primarily transverse magnetic perturbations, $\delta\mathbf{B}$ is well described by one function $\alpha(\psi_p, \theta, \zeta, t)$, in the form:

$$\delta\mathbf{B} = \nabla \times \alpha\mathbf{B} = \nabla \times \delta\mathbf{A} \tag{3}$$

Now, let $\rho_\parallel = v_\parallel/\Omega$, with Ω being the particle's gyro-frequency, then the canonical momenta for the particle's guiding center are given by:

$$P_\zeta = \frac{e}{c}[g(\rho_\parallel + \alpha) - \psi_p] = \frac{e}{c}[g\rho_c - \psi_p]$$

$$P_\theta = \frac{e}{c}[I(\rho_\parallel + \alpha) + \psi_t] = \frac{e}{c}[I\rho_c + \psi_t] \tag{4}$$

with ψ_t the toroidal flux. Finally, let ϕ be the perturbed electric potential, the particle's Hamiltonian is then:

$$\mathcal{H} = \frac{e^2B^2}{2mc^2}(\rho_c - \alpha)^2 + \mu B + e\phi \tag{5}$$

Therefore, we have the Hamiltonian guiding center equations:

$$\dot{P}_\zeta = -\frac{\partial\mathcal{H}}{\partial\zeta}, \qquad \dot{\zeta} = \frac{\partial\mathcal{H}}{\partial P_\zeta}$$

$$\dot{P}_\theta = -\frac{\partial\mathcal{H}}{\partial\theta}, \qquad \dot{\theta} = \frac{\partial\mathcal{H}}{\partial P_\theta} \tag{6}$$

Substitute $(\dot{P}_\zeta, \dot{P}_\theta)$ with $(\dot{\psi}_p, \dot{\rho}_\parallel)$ by solving Eqs. 4, and we obtain the set of differential equations actually used in the code:

$$\dot{\psi}_p = \frac{1}{D}\Bigg\{ - I\left[-\left(\mu + \frac{e^2\rho_\parallel^2}{mc^2}B\right)\frac{\partial B}{\partial \zeta} + \frac{e^2B^2}{mc^2}\rho_\parallel\frac{\partial \alpha}{\partial \zeta} - e\frac{\partial \phi}{\partial \zeta}\right] + \\ + g\left[-\left(\mu + \frac{e^2\rho_\parallel^2}{mc^2}B\right)\frac{\partial B}{\partial \theta} + \frac{e^2B^2}{mc^2}\rho_\parallel\frac{\partial \alpha}{\partial \theta} - e\frac{\partial \phi}{\partial \theta}\right]\Bigg\} \tag{7}$$

$$\dot{\theta} = \frac{1}{D}\Bigg\{(1 - \rho_c g')\frac{e^2B^2}{mc^2}\rho_\parallel + \\ + g\left[\left(\mu + \frac{e^2\rho_\parallel^2}{mc^2}B\right)\frac{\partial B}{\partial \psi_p} - \frac{e^2B^2}{mc^2}\rho_\parallel\frac{\partial \alpha}{\partial \psi_p} + e\frac{\partial \phi}{\partial \psi_p}\right]\Bigg\} \tag{8}$$

$$\dot{\zeta} = \frac{1}{D}\Bigg\{(q + \rho_c I')\frac{e^2B^2}{mc^2}\rho_\parallel - \\ - I\left[\left(\mu + \frac{e^2\rho_\parallel^2}{mc^2}B\right)\frac{\partial B}{\partial \psi_p} - \frac{e^2B^2}{mc^2}\rho_\parallel\frac{\partial \alpha}{\partial \psi_p} + e\frac{\partial \phi}{\partial \psi_p}\right]\Bigg\} \tag{9}$$

$$\dot{\rho}_\parallel = -\frac{1}{D}\Bigg\{(q + \rho_c I' + I\frac{\partial \alpha}{\partial \psi_p})\left[\left(\mu + \frac{e^2\rho_\parallel^2}{mc^2}B\right)\frac{\partial B}{\partial \zeta} + e\frac{\partial \phi}{\partial \zeta}\right] + \\ + (1 - \rho_c g' - g\frac{\partial \alpha}{\partial \psi_p})\left[\left(\mu + \frac{e^2\rho_\parallel^2}{mc^2}B\right)\frac{\partial B}{\partial \theta} + e\frac{\partial \phi}{\partial \theta}\right] + \\ + (g\frac{\partial \alpha}{\partial \theta} - I\frac{\partial \alpha}{\partial \zeta})\left[\left(\mu + \frac{e^2\rho_\parallel^2}{mc^2}B\right)\frac{\partial B}{\partial \psi_p} + e\frac{\partial \phi}{\partial \psi_p}\right]\Bigg\} - \frac{\partial \alpha}{\partial t} \tag{10}$$

Where,

$$D = \frac{e}{c}[gq + I + \rho_c(gI' - Ig')] \tag{11}$$

and primes refer to derivatives with respect to ψ_p. The above equations describing the Hamiltonian guiding center motion are incorporated into the code ORBIT.[11–13]

III. Sawtooth Mode Structure

Since most TFTR plasmas have circular cross section, and sawtooth activities are dominant within the $q(r_s) = 1$ flux surface, with r_s satisfying $r_s/R \ll 1$, the mode structure in the cylindrical limit is a good approximation. Near the $q = 1$ flux surface in a typical TFTR discharge, the resistive time and Alfvén time are $\tau_R \simeq 88$ sec and $\tau_A \simeq 4.0 \times 10^{-7}$ sec respectively. Therefore the magnetic Reynolds number is $S = \tau_R/\tau_A \simeq 2.2 \times 10^8 \gg 1$, corresponding to the ideal magnetohydrodynamic (MHD) limit. In this limit, the actual sawtooth mode shape is well approximated by that of the ideal MHD sawtooth mode. For an ideal MHD eigenmode m/n, with ξ_{0mn} the perturbation magnitude at $q = m/n$ flux surface, we have

$$\begin{aligned}\alpha_{mn} &= \frac{r\xi_{0mn}}{R_0}\left(\frac{r}{r_s}\right)^{(m-1)}\left(\frac{1}{q} - \frac{n}{m}\right)\cos(n\zeta - m\theta - \omega t)H\left(\frac{m}{n} - q\right) \\ &= \frac{r\xi_0}{R_0}\left(\frac{r}{r_s}\right)^{(m-1)}\left(\frac{1}{q} - \frac{n}{m}\right)\mathrm{Re}[e^{i(n\zeta - m\theta - \omega t)}]H\left(\frac{m}{n} - q\right) \qquad (12)\end{aligned}$$

with H the Heavyside step function. Fig. 1 shows the mode structure of a typical TFTR case, with 1/1 and 2/1 modes present. For numerical reasons the Heavyside functions are made smooth, so that they possess continuous derivatives, as we will discuss below. This smoothing is equivalent to the inclusion of the effects of a small but nonzero resistivity. Because of the highly peaked nature of the alpha distribution the mode structure is irrelevant much beyond the $q = 1$ surface, so in fact this smoothing is important only for the $m = 1$ harmonic.

Parameters of a typical TFTR equilibrium are shown in Table 1:

Table 1: Parameters of a typical TFTR equilibrium

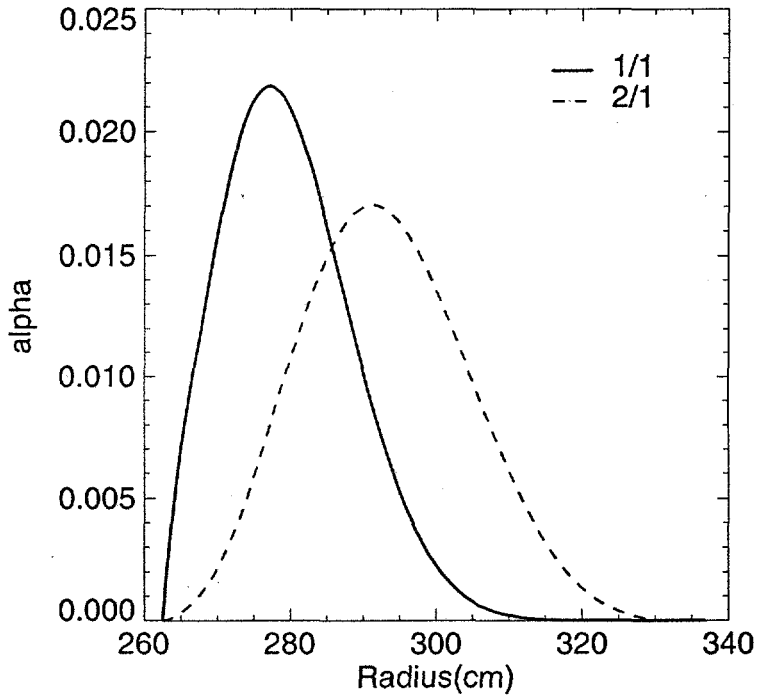

Figure 1: Mode structure for TFTR run #84549 @ t= 4.4 sec. The frequency of saw-tooth oscillation is $\omega = 7.68kHz$. The peak value of α corresponds to the perturbed magnetic field of the order : $|\delta \mathbf{B}/B| \sim \alpha/a_0 \sim 2.5\%$.

B_0	$5.0T$	I_0	2.0 MA
R_0	$260.0cm$	a	$90.0cm$
q_0	0.8	q_w	3.5

Let $\xi_0 = r_s(q = 1) = 25.0cm$, the parameters for sawtooth modes are shown in Table 2:

Table 2: Values for different modes

Mode	Rational Surface	$(\|\delta \mathbf{B}\|/B_0)_{\max}$	$\alpha_{\max}(cm)$	Frequency (rad/sec)
1/1	25.0 cm	0.0236	0.206	7.54×10^3
4/3	40.0 cm	0.0413	0.318	5.78×10^4
2/1	60.0 cm	0.953	1.559	2.0×10^4

The sawtooth mode frequencies, determined by local diamagnetic effects, are given by experimental measurements.[14] To determine the peak value of the sawtooth modes, we plot the Poincaré cross section of the magnetic field in the presence of two sawtooth modes and scan through the magnitudes of the perturbations. When the Poincaré plot shows a significant degree of stochasticity, indicating the onset of full magnetic reconnection, we choose that set of perturbation magnitudes as the peak values for the modes. This procedure is subjective to some extent, but the results were not sensitive to the exact value of the magnitudes as long as the threshold for full reconnection is reached. Fig. 2 shows the Poincaré plot of the magnetic field in the presence of the two sawtooth modes shown in Fig. 1. At the peak values of magnitude of the sawtooth oscillations, the topology of the magnetic flux surfaces are totally destroyed

by the nonlinear interaction of the two modes near the central region of the plasma.

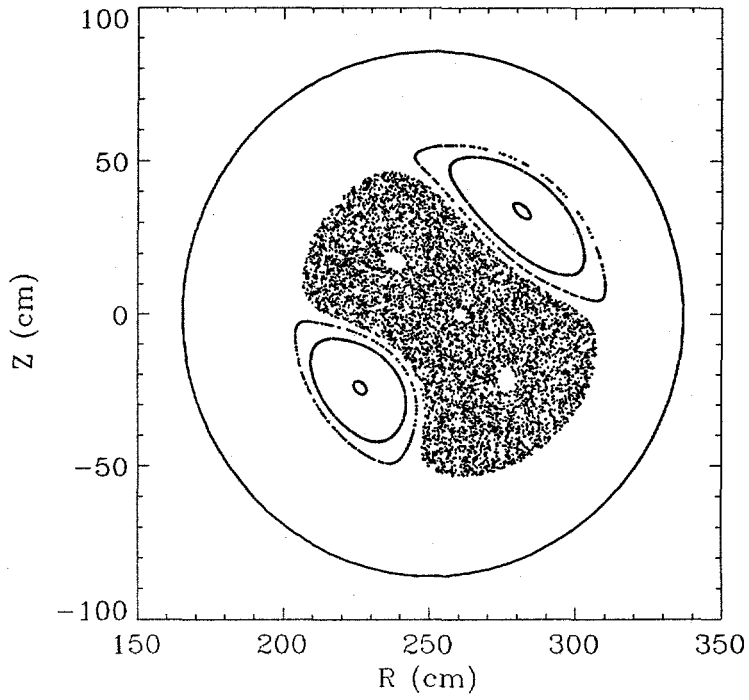

Figure 2: Poincaré plot for magnetic field lines.. *Two sawtooth modes are present with* $\xi_0(1/1) = 1.0 r_s(1/1)$, *and* $\xi_0(2/1) = 0.4 r_s(2/1)$.

IV. The Perturbation Induced Electric Field

To determine when the perturbation induced electric field is important, it is necessary to look at the time scales of bounce motion of trapped and passing particles. Fig. 3 shows how the poloidal bounce period of a 1 MeV α particle varies with its pitch angle (at the mid-plane) and poloidal flux. The tips, corresponding to the

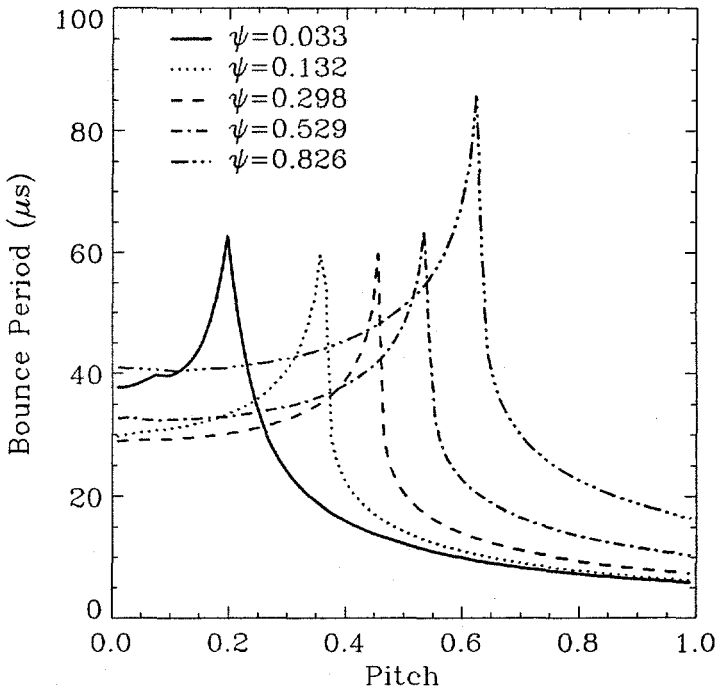

Figure 3: Alpha particle's bounce period. $E = 1MeV$. TFTR run 86644 at t= 4.35 sec. The pitch is measured at mid-plane. ψ is the normalized poloidal flux..

trapped-passing boundary, are actually infinite, but numerical resolution truncates them as shown. Since the typical crash time for a sawtooth in TFTR is of the order $\tau_{cr} \sim 15\mu sec$, and the passing particle transit time is about $10\mu sec$, the perturbed electric field is closer to resonance with trapped particles than with passing particles. In addition, energy is transfered to the particles through $\mathbf{E} \cdot \mathbf{V}_d$, with $\mathbf{V}_d$ the cross field drift motion, much larger for trapped than for passing particles.

The perturbed electric potential can be written as a sum of Fourier components:

$$\phi(\psi_p, \theta, \zeta, t) = \sum_{\mathrm{m,n}} \phi_{\mathrm{mn}}(\psi_p, t) e^{i(n\zeta - m\theta - \omega t)} \tag{13}$$

Since ideal MHD is valid in the time scale of interest, the parallel electric field must be shorted out by electrons,

$$E_\parallel = \hat{\mathbf{b}} \cdot \left(\nabla\phi - \frac{\partial \mathbf{A}}{\partial t}\right) = \hat{\mathbf{b}} \cdot \left(\nabla\phi - \frac{\partial(\alpha \mathbf{B})}{\partial t}\right) = 0 \tag{14}$$

by using

$$\mathbf{B} \cdot \nabla = \frac{1}{\mathcal{J}}\left(\frac{\partial}{\partial\theta} + q\frac{\partial}{\partial\zeta}\right)$$

we have:

$$\hat{\mathbf{b}} \cdot \nabla\phi = \frac{1}{B\mathcal{J}} \sum_{\mathrm{m,n}} i(nq - m)\phi_{\mathrm{m,n}}(\psi_p, t) e^{i(n\zeta - m\theta - \omega t)} \tag{15}$$

Noting that

$$\hat{\mathbf{b}} \cdot \frac{\partial(\alpha \mathbf{B})}{\partial t} = B\frac{\partial \alpha}{\partial t}$$

$$\frac{\partial \alpha}{\partial t} = \sum_{\mathrm{m,n}} \left(\frac{\partial \alpha_{\mathrm{mn}}}{\partial t} - i\omega\alpha_{\mathrm{mn}}\right) e^{i(n\zeta - m\theta - \omega t)} \tag{16}$$

Combining the above equations, we arrive at:

$$\phi_{\mathrm{mn}}(\psi_p, t) = \frac{(gq + I)}{(m - nq)}\left(\omega\alpha_{\mathrm{mn}} + i\frac{\partial \alpha_{\mathrm{mn}}}{\partial t}\right) \tag{17}$$

For the purpose of implementation into the code, it is more convenient to relate ϕ_{mn} directly to ξ_{0mn}, the displacement corresponding to mode (m/n). In cylindrical approximation:

$$\phi_{\mathrm{mn}}(\psi_p, t) = i\Big(\frac{r}{m}\Big)\Big(\frac{r}{r_s}\Big)^{m-1}\Big(i\omega\xi_{0\mathrm{mn}} + \frac{\partial\xi_{0\mathrm{mn}}}{\partial t}\Big)H\Big(\frac{m}{n} - q\Big) \tag{18}$$

Its derivative with respect to ψ_p is then:

$$\frac{\partial\phi_{\mathrm{mn}}(\psi_p, t)}{\partial\psi_p} = i\Big(\frac{q}{r}\Big)\Big(\frac{r}{r_s}\Big)^{m-1}\Big(i\omega\xi_{0\mathrm{mn}} + \frac{\partial\xi_{0\mathrm{mn}}}{\partial t}\Big)H\Big(\frac{m}{n} - q\Big) +$$

$$+i\Big(\frac{q}{m}\Big)\Big(\frac{r}{r_s}\Big)^{m-1}\Big(i\omega\xi_{0\mathrm{mn}} + \frac{\partial\xi_{0\mathrm{mn}}}{\partial t}\Big)\frac{d}{dr}\Big[H\Big(\frac{m}{n} - q\Big)\Big] \tag{19}$$

Obviously, this derivative is singular at the rational surface, since the derivative of a step function is a δ-function! The singularity is due to our simplified assumption of the ideal MHD limit and does not correctly represent the actual potential. Since resistivity is non zero, a magnetic island forms due to the perturbation. Inside the island, flux surfaces close on themselves and modify the potential. As a first approximation we take the electric potential to be flat around the rational surface within the range of island width, rather than having a singularity as given by Eq. 19. The island width (in terms of poloidal flux), is given by

$$\Delta\psi_p = \frac{4m}{n}\Big(\frac{g\alpha_0}{q'}\Big)^{1/2} \propto \sqrt{\alpha_0} \tag{20}$$

and increases with the magnitude of the perturbation which evolves with time. We smooth the potential within the range of the island width around the rational surface, thus avoiding the singularity.

By imposing the condition of $E_\parallel = 0$, the last component of the guiding center equations, Eq. 10 is modified as:

$$\dot{\rho_\parallel} = -\frac{\partial \alpha}{\partial t} + \frac{1}{D}\Bigg\{ -(\rho_c I' + q)e\frac{\partial \phi}{\partial \zeta} - (1 - \rho_c g')e\frac{\partial \phi}{\partial \theta} +$$

$$+ \left(\mu + \frac{e^2\rho_\parallel^2}{mc^2}B\right)\left[(\rho_c g' - 1) + g\left(\frac{\partial \alpha}{\partial \psi_p}\frac{\partial B}{\partial \theta} - \frac{\partial \alpha}{\partial \theta}\frac{\partial B}{\partial \psi_p}\right) + I\frac{\partial \alpha}{\partial \zeta}\frac{\partial B}{\partial \psi_p}\right] +$$

$$+ e\left[g\left(\frac{\partial \alpha}{\partial \psi_p}\frac{\partial \phi}{\partial \theta} - \frac{\partial \alpha}{\partial \theta}\frac{\partial \phi}{\partial \psi_p}\right) + I\left(\frac{\partial \alpha}{\partial \zeta}\frac{\partial \phi}{\partial \psi_p} - \frac{\partial \alpha}{\partial \psi_p}\frac{\partial \phi}{\partial \zeta}\right)\right]\Bigg\} \qquad (21)$$

V. Evolution of Sawtooth Modes

Not much detailed information is provided by the current experimental observations concerning the temporal evolution of a sawtooth cycle. Thus we take as a model the simplest approximation, in which a sawtooth crash cycle can be characterized by two time scales—one describing the relatively slow build-up of amplitudes and the other describing the sudden decline. A sawtooth crash cycle generally starts with a single mode (in our case, the $m/n = 1/1$ mode) of small amplitude. This single mode grows exponentially with time, until its magnitude becomes large enough to excite other nearby modes (such as the 2/1 and 4/3 modes). All modes continue to grow until their nonlinear interaction leads to a flattening of the current density and temperature profiles followed by a rapid crash to zero magnitude of the perturbation, concluding a sawtooth cycle. We model this evolution using the following

parameterized analytic form.

$$\xi(t) = \begin{cases} \xi_0(\exp\left(\frac{t}{\tau_1}\right) - 1)/(e-1), & \text{for } t < \tau_1, \\ \xi_0(\exp\left(\frac{t-\tau_1-\tau_2}{\tau_2}\right) - 1)/(e-1), & \text{for } \tau_1 < t < \tau_1 + \tau_2. \end{cases} \tag{22}$$

where $\tau_2 \ll \tau_1$. We adjust τ_1 and τ_2 for each mode according to experimental data. The crash time, τ_2, is much slower than the cyclotron rotation of the particles, thus the conservation of magnetic moments is valid even in the crash phase. But τ_2 is of comparable magnitude with the trapped particle bounce period and a partial resonance causes the particles to diffuse in velocity space. A typical case of temporal evolution is shown in Fig. 4.

VI. Monte Carlo Simulation of Alpha Distributions

In order to make sensible comparison with experimental measurements, it is important to interpret the output of the Monte Carlo simulations properly, and to understand how the output would correspond to measurements from the PCX and α-CHERS diagnostics. In fact, the correspondence can be quite subtle for the PCX case.

Let $F(\psi_p, E, \mu)$ be the particle distribution in the phase space $(\mathbf{x}, \mathbf{v})$, and $\mathcal{F}(\psi_p, E, \mu)$ be the counter part in the phase space of $(\psi_p, \theta, E, \lambda)$. (λ is the mid-plane pitch and has a one-to-one correspondence with magnetic moment μ). Note that,

$$d^3x d^3v = 4\pi^2 \sqrt{E} \mathcal{J} d\psi_p d\theta d\lambda dE \tag{23}$$

with, $\mathcal{J}$ the Jacobian of the flux coordinate system. The number of particles per unit

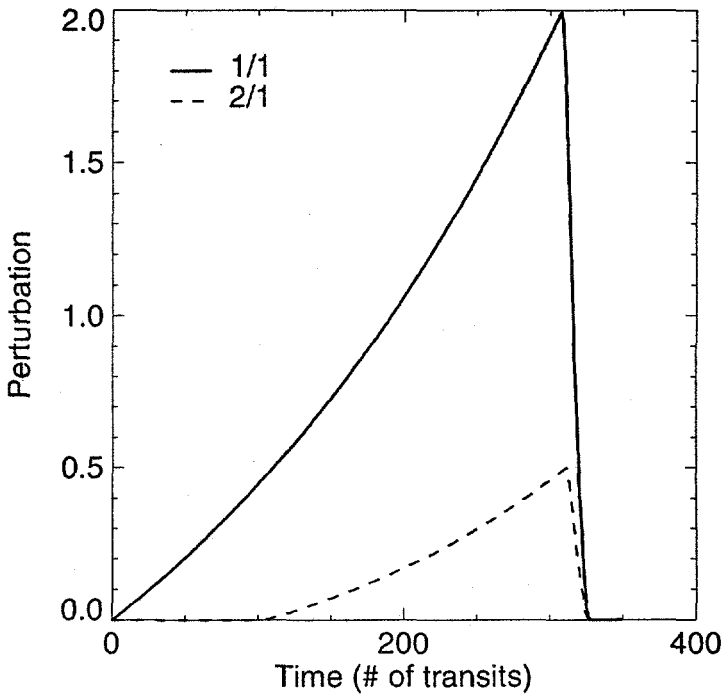

Figure 4: Evolution of sawtooth amplitudes for 1/1 and 2/1 modes.. *The duration of one sawtooth crash cycle is* $\sim 2.3msec$. *The crash time is of the order:* $\tau_{\text{crash}} \sim 15\mu sec$.

phase space volume is,

$$dN = F(\psi_p, E, \mu) d^3x d^3v = \mathcal{F}(\psi_p, E, \mu) d\psi_p d\theta d\lambda dE \tag{24}$$

Therefore,

$$\mathcal{F}(\psi_p, E, \mu) = 4\pi^2 \sqrt{E} \mathcal{J} F(\psi_p, E, \mu) \tag{25}$$

For the case of a Gaussian radial distribution, $n(r) = n_0 \exp(-(r/h)^2)$, the peakedness is determined by the single parameter h. Fig. 5 shows an example of how well the Monte Carlo generated particle distribution represents the intended analytic distribution.

VII. Comparison with Experiments

The α-CHERS experiment was performed in a standard TFTR D-T super-shot with toroidal magnetic field of 5.1T, and major and minor radii of $R = 2.52m$ and $a = 0.87m$, respectively. This diagnostic measures the alpha particles with energies in the 0.15-0.6 MeV range and positive pitch angles (with $\lambda \in [0, 1]$ and mostly passing particles). We modeled the alpha radial density profile before the sawtooth crash using a fit obtained from TRANSP analysis.[15]

$$n(r) = n_0 (1 - (\frac{r}{a})^2)^9 \tag{26}$$

The initial pitch distribution was taken to be uniform in the range of $[0, 1]$. After the crash, the particle's radial density profile is reconstructed by statistical analysis. Fig. 6 shows the simulation of the redistribution of passing particles with $0.15MeV < E < 0.6MeV$. The results are seen to be in reasonable agreement with the experiment.

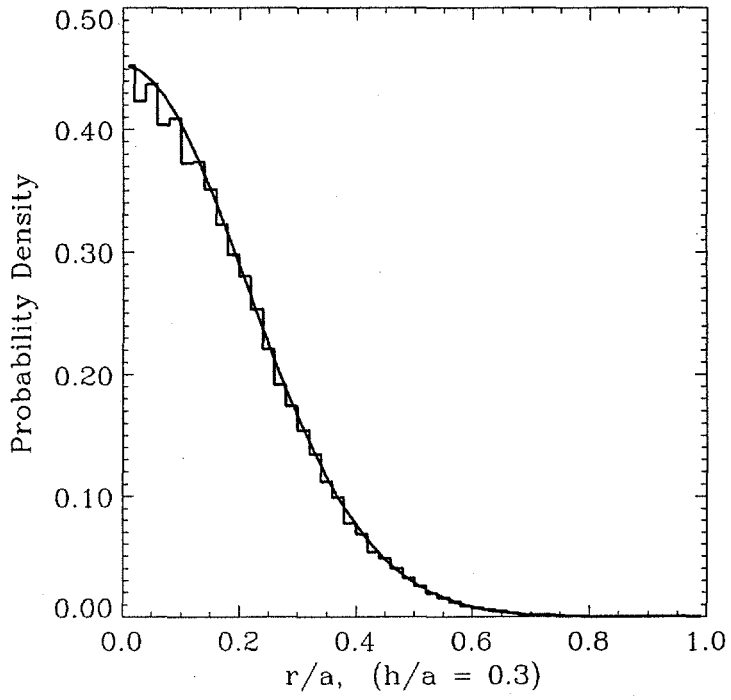

Figure 5: The Gaussian distribution $f(r) \propto \exp(-(r/h)^2)$ (smooth curve) is simulated by Monte Carlo method (histogram). *40000 particles are used. The peakedness parameter is* $h = 0.3a$.

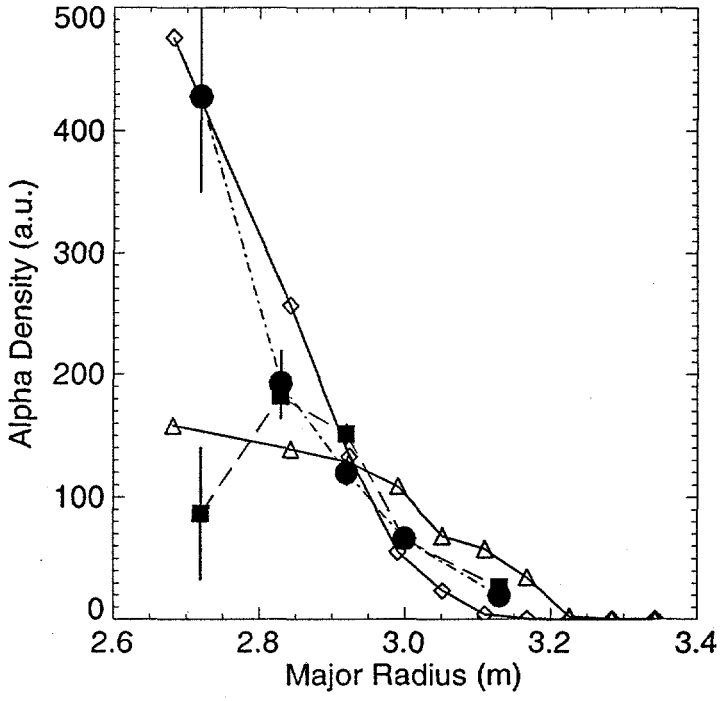

Figure 6: The results from α-CHERS measurements are the ones with error bars. Solid circles are pre-crash measurements and squares are the post-crash measurements. Simulation of the α-CHERS diagnostics are the solid lines with the diamonds indicating pre-crash density and triangles the post-crash density.

We found that to simulate PCX diagnostics is more subtle. The PCX diagnostic measures alpha particles with one single energy value at a time, with $0.8MeV \leq E \leq 1.21MeV$. Furthermore, only deeply trapped particles with pitch $\lambda = -0.048 \pm 0.001$ are detected. It is easy to launch particles with a single value of pitch angle, but it is statistically impossible to collect an acceptably large number of particles which happen to be within a narrow range of pitch angle after the sawtooth crash. Among the particles we launched at the beginning, all of which satisfying the criteria to be picked up by the detector, about only half of them still satisfy that criteria at the end of a sawtooth cycle. At the moment, we have to sacrifice accuracy for better statistics by widening the range of acceptable pitch angles. Comparisons between the experimental measurements and our simulations are displayed in Fig. 7, 8 and 9 for three different energies. Although the results are not as clear as in the case of the α-CHERS simulation, both experiment and simulation show a broadening of the particle distribution by roughly 10 cm.

A picture of the trapped particle motion will help us to understand this result. A trapped particle passes the outer mid-plane twice in each bounce-period, with smaller minor radius when passing with negative pitch angle and larger minor radius with positive pitch angle. One mechanism for the depletion of the particles with small negative pitches is induced transition by the mode into passing particles during the positive pitch angle phase of the orbit (*i.e.* while they are relatively further away from the magnetic axis). This would require only a small resonant energy transfer to the particle. Supporting evidence is provided by a similar simulation in which we

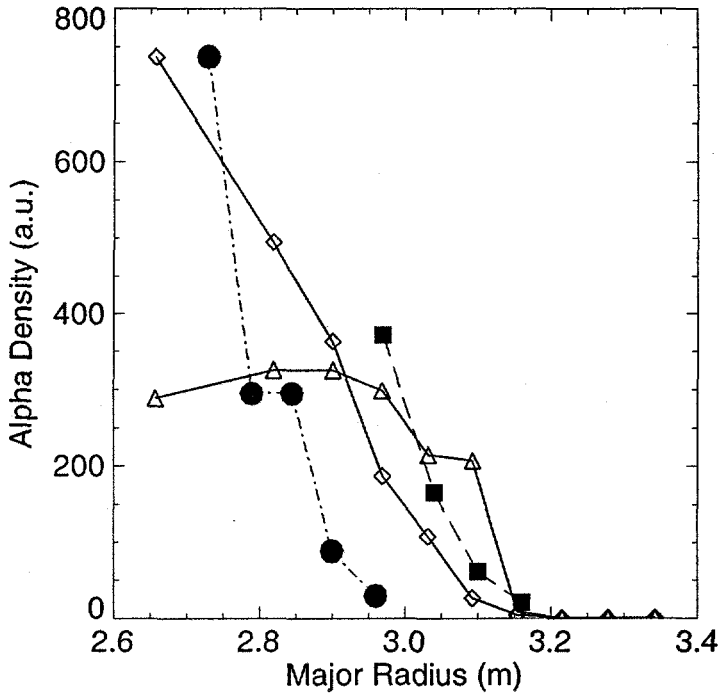

Figure 7: TFTR run #84549 @ t= 4.4 sec, E = 0.8 MeV, PCX, pre-crash measurements are solid circles and post-crash are solid squares. The simulations are in solid line: diamonds are pre-crash and triangles are post-crash.. *Duration of the sawtooth cycle is 2.6 msec. Mid-plane pitch range:* $\lambda \in [-0.4, 0.0]$.

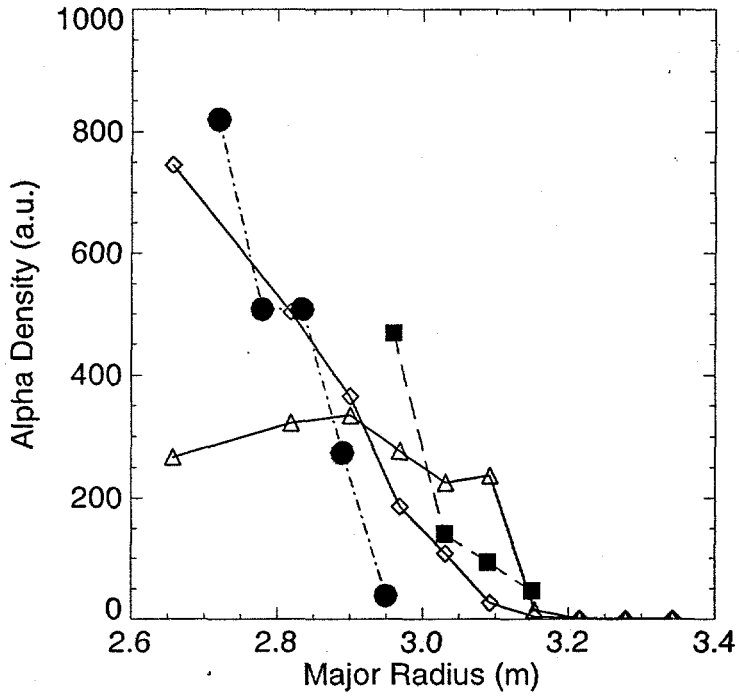

Figure 8: TFTR run #84549 @ t= 4.4 sec, E = 1.0 MeV, PCX, pre-crash measurements are solid circles and post-crash are solid squares. The simulations are in solid line: diamonds are pre-crash and triangles are post-crash.. *Duration of sawtooth cycle is 2.6 msec. Mid-plane pitch range:* $\lambda \in [-0.4, 0.0]$.

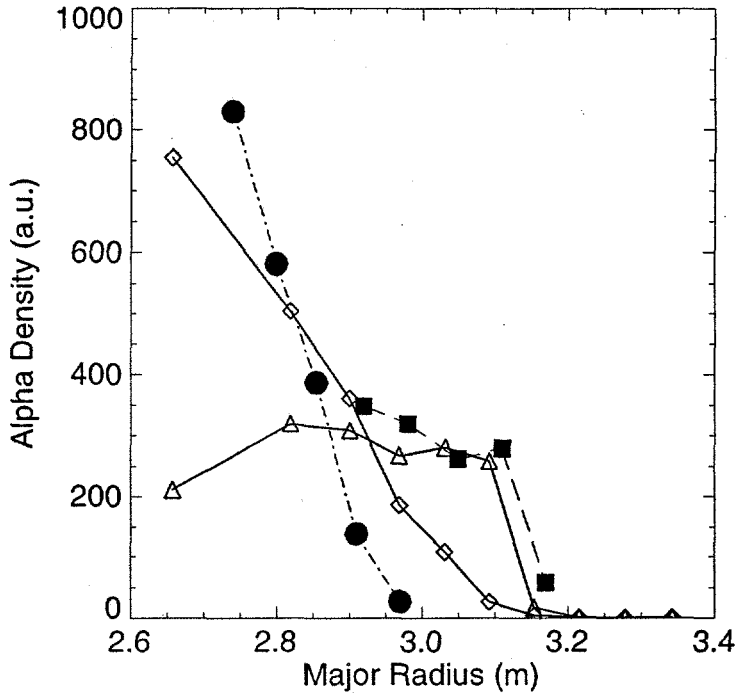

Figure 9: TFTR run #84549 @ t= 4.4 sec, E = 1.21 MeV, PCX, pre-crash measurements are solid circles and post-crash are solid squares. The simulations are in solid line: diamonds are pre-crash and triangles are post-crash.. *Duration of the sawtooth cycle is 2.6 msec. Mid-plane pitch range:* $\lambda \in [-0.4, 0.0]$.

find that the number of particles with small but positive pitch is increased by the sawtooth crash cycle.

We do not see any significant loss of particles throughout our simulations.

VIII. Conclusion

A numerical model based on the Hamiltonian guiding center equations has been developed for the analysis of the sawtooth mixing phenomena in TFTR D-T experiments. There are two important processes in the α particle redistribution: the stochasticity of magnetic field lines at peak perturbation amplitudes, and the large perpendicular electric field during the sawtooth crash. The simulations for passing particles with positive mid-plane pitch angles are in good agreement with the α-CHERS results. The simulations corresponding to PCX measurements suffer from poor statistics and possibly incorrect treatment of the electric field in the nonlinear stage. An improved model for the sawtooth crash would possibly allow more detailed comparisons.

Acknowledgments

We are glad to thank R. V. Budny, Z. Chang, N. N. Gorelenkov, J. Manickam, M. Petrov and B. Stratton for their interest and help in this work. This work was supported by the U.S. Department of Energy Contract No. DE-AC02-76-CHO-3073.

References

[1]R. Hawryluk et al., Plasma Phys. Controlled Fusion **33**, 1509 (1991).

[2]R. K. Fisher et al., Phys. Rev. Lett. **75**, 846 (1995).

[3]M. P. Petrov, H. H. Duong, R. K. Fisher, N. N. Gorelenkov, and S. S. Medley, Nucl. Fusion **35**, 1437 (1995).

[4]M. P. Petrov, R. V. Budny, H. H. Duong, and et al., PPPL Report **3121** (1995).

[5]G. McKee et al., Phys. Rev. Lett. **75**, 649 (1995).

[6]D. Anderson, Y. I. Kolesnichenko, M. Lisak, F. Wising, and Y. V. Yakovenko, Nucl. Fusion **34**, 217 (1994).

[7]V. Y. Goloborod'ko, Y. I. Kolesnichenko, and V. A. Yavorskij, Physica Scripta, **T16** , 46 (1987).

[8]N. N. Gorelenkov et al., PPPL Report **3184** (1996).

[9]S. J. Zweben et al., Nucl. Fusion **35**, 1445 (1995).

[10]R. B. White, A. H. Boozer, and R. Hay, Phys. Fluids **25**, 575 (1982).

[11]R. B. White and M. S. Chance, Phys. Fluids **27**, 2445 (1984).

[12]R. B. White, Phys. Fluids B **2**, 845 (1990).

[13]R. B. White, *Theory of Tokamak Plasmas*, North Holland, 1989.

[14]Z. Chang et al., Phys. Rev. Lett. **74**, 4663 (1995).

[15]R. V. Budny, Nucl. Fusion **34**, 1247 (1994).